# A reconstruction method for cone-beam differential x-ray phase-contrast computed tomography

**Jian Fu,**[1,*] **Astrid Velroyen,**[2] **Renbo Tan,**[1] **Junwei Zhang,**[1] **Liyuan Chen,**[1] **Arne Tapfer,**[2] **Martin Bech,**[2,3,4] **and Franz Pfeiffer**[2]

[1]*Beijing University of Aeronautics and Astronautics, 100191 Beiijng, China*
[2]*Technische Universität München, 85748 Garching, Germany*
[3]*Lund University, 221 85 Lund, Sweden*
[4]*martin.bech@tum.de*
[*]*fujian706@buaa.edu.cn*

**Abstract:** Most existing differential phase-contrast computed tomography (DPC-CT) approaches are based on three kinds of scanning geometries, described by parallel-beam, fan-beam and cone-beam. Due to the potential of compact imaging systems with magnified spatial resolution, cone-beam DPC-CT has attracted significant interest. In this paper, we report a re-construction method based on a back-projection filtration (BPF) algorithm for cone-beam DPC-CT. Due to the differential nature of phase contrast projections, the algorithm restrains from differentiation of the projection data prior to back-projection, unlike BPF algorithms commonly used for absorption-based CT data. This work comprises a numerical study of the algorithm and its experimental verification using a dataset measured with a three-grating interferometer and a micro-focus x-ray tube source. Moreover, the numerical simulation and experimental results demonstrate that the proposed method can deal with several classes of truncated cone-beam datasets. We believe that this feature is of particular interest for future medical cone-beam phase-contrast CT imaging applications.

## References and links

1. R. Fitzgerald, "Phase-sensitive x-ray imaging," Phys. Today **7**, 23–26 (2000).
2. A. Momose, "Recent advances in x-ray phase imaging," Jpn. J. Appl. Phys. **44**, 6355–6367 (2005).
3. F. Pfeiffer, C. David, O. Bunk, T. Donath, M. Bech, G. Le Duc, A. Bravin, and P. Cloetens, "Region-of-interest tomography for grating-based differential phase-contrast imaging," Phys. Rev.Lett. **101**, 168101 (2008).
4. C. Raven, A. Snigirev, I. Snigireva, P. Spanne, A. Souvorov, and V. Kohn, "Phase-contrast microtomography with coherent high-energy synchrotron x rays," Appl. Phys. Lett. **69**, 1826–1828 (1996).
5. F. Beckmann, K. Heise, B. Kolsch, U. Bonse, M. Rajewsky, and T. Biermann, "Three-dimensional imaging of nerve tissue by x-ray phase-contrast microtomography," Biophys. J. **76**, 98–102 (1999).
6. P. Cloetens, W. Ludwig, J. Baruchel, D. van Dyck, J. van Landuyt, J. P. Guigay, and M. Schlenker, "Holotomography:quantitative phase tomography with micrometer resolution using hard synchrotron radiation x rays," Appl. Phys. Lett. **75**, 2912–2914 (1999).
7. F. A. Dilmanian, Z. Zhong, B. Ren, X. Y. Wu, L. D. Chapman, I. Orion, and W. C. Thomlinson, "Computed tomography of x-ray index of refraction using the diffraction enhanced imaging method," Phys. Med.Biol. **45**, 933–946 (2000).

8. S. C. Mayo, T. J. Davis, T. E. Gureyev, P. R. Miller, D. Paganin, A. Pogany, A. W. Stevenson, and S. W. Wilkins, "X-ray phase-contrast microscopy and microtomography," Opt. Express **11**, 2289–2302 (2003).

9. P. J. McMahon, A. G. Peele, D. Paterson, J. J. A. Lin, T. H. K. Irving, I. McNulty, and K. A. Nugent, "Quantitative x-ray phase tomography with sub-micron resolution," Opt. Commun. **217**, 53–58 (2003).

10. A. Momose, S. Kawamoto, I. Koyama, Y. Hamaishi, K. Takai, and Y. Suzuki, "Demonstration of x-ray talbot interferometry," Jpn. J. Appl. Phys. **42**, L866–L868 (2003).

11. T. Weitkamp, A. Diaz, C. David, F. Pfeiffer, M. Stampanoni, P. Cloetens, and E. Ziegler, "X-ray phase imaging with a grating interferometer," Opt. Express **13**, 6296–6304 (2005).

12. A. Groso, M. Stampanoni, R. Abela, P. Schneider, S. Linga, and R. Müller, "Phase contrast tomography: an alternative approach," Appl. Phys. Lett. **88**, 214104 (2006).

13. A. Momose, W. Yashiro, Y. Takeda, Y. Suzuki, and T. Hattori, "Phase tomography by x-ray talbot interferometry for biological imaging," Jpn. J. Appl. Phys. **45**, 5254–5262 (2006).

14. A. Bravin, J. Keyrilainen, M. Fernandez, S. Fiedler, C. Nemoz, M. L. Karjalainen-Lindsberg, M. Tenhunen, P. Virkkunen, M. Leidenius, K. V. Smitten, P. Sipila, and P. Suortti, "High-resolution ct by diffraction-enhanced x-ray imaging: mapping of breast tissue samples and comparison with their histo-pathology," Phys. Med. Biol. **52**, 2197–2211 (2007).

15. F. Pfeiffer, M. Bech, O. Bunk, P. Kraft, E. F. Eikenberry, C. Brönnimann, C. Grünzweig, and C. David, "Hard-x-ray dark-field imaging using a grating interferometer," Nature Mater. **7**, 134 (2008).

16. F. Pfeiffer, C. Kottler, O. Bunk, and C. David, "Hard x-ray phase tomography with low-brilliance sources," Phys. Rev. Lett. **98**, 108105 (2007).

17. M. Bech, T. H. Jensen, R. Feidenhans'l, O. Bunk, C. David, and F. Pfeiffer, "Soft-tissue phase-contrast tomography with an x-ray tube source," Phys. Med. Biol. **54**, 2747–2753 (2009).

18. F. Pfeiffer, T. Weitkamp, O. Bunk, and C. David, "Phase retrieval and differential phase-contrast imaging with low-brilliance x-ray sources," Nat. Phys. **2**, 258–261 (2006).

19. P. P. Zhu, K. Zhang, Z. L. Wang, Y. J. Liu, X. S. Liu, Z. Y. Wu, S. A. McDonald, F. Marone, and M. Stampanoni, "Low-dose, simple, and fast grating-based x-ray phase-contrast imaging," Proc. Natl Acad. Sci. USA **107**, 13576–13581 (2010).

20. M. Takeda, H. Ina, and S. Kobayashi, "Fourier-transform method of fringe-pattern analysis for computer-based topography and interferometry," J. Opt. Soc. Am. **72**, 156–160 (1982).

21. I. Jerjen, V. Revol, C. Kottler, T. Luethi, U. Sennhauser, R. Kaufmann, and C. Urban, "Phase contrast cone beam tomography with an x-ray grating interferometer," AIP Conf. Proc. **1236**, 227–231 (2010).

22. T. G. Zhuang, S. Leng, B. E. Nett, and G. H. Chen, "Fan-beam and cone-beam image reconstruction via filtering the backprojection image of differentiated projection data," Phys. Med. Biol. **49**, 5489–5503 (2004).

23. F. Noo, R. Clackdoyle, and J. D. Pack, "A two-step Hilbert transform method for 2D image reconstruction," Phys. Med. Biol. **49**, 3903–3923 (2004).

24. S. Leng, T. G. Zhuang, B. E. Nett, and G. H. Chen, "Exact fan-beam image reconstruction algorithm for truncated projection data acquired from an asymmetric half-size detector," Phys. Med. Biol. **50**, 1805–1820 (2005).

25. X. Pan, Y. Zou, and D. Xia, "Image reconstruction in peripheral and central regions-of-interest and data redundancy," Med. Phys. **32**, 673–684 (2005).

26. G. H. Chen and Z. Qi, "Image reconstruction for fan-beam differential phase contrast computed tomography," Phys. Med. Biol. **53**, 1015–1025 (2008).

27. J. Fu, P. Li, Q. Wang, S. Wang, M. Bech, A. Tapfer, D. Hahn, and F. Pfeiffer, "A reconstruction method for equidistant fan-beam differential phase contrast computed tomography," Phys. Med. Biol. **56**, 4259–4238 (2011).

28. A. C. Kak and M. Slaney, *Principles of Computerized Tomography* (IEEE Press, 1987).

29. A. Tapfer, M. Bech, B. Pauwels, X. Liu, P. Bruyndonckx, A. Sasov, J. Kenntner, J. Mohr, M. Walter, J. Schulz, and F. Pfeiffer, "Development of a prototype gantry system for preclinical x-ray phase-contrast computed tomography," Med. Phys. **38**, 5910–5915 (2011).

---

## 1. Introduction

X-ray phase-contrast computed tomography (PC-CT) uses the phase shift that x-rays undergo when passing through matter, rather than their attenuation, as the imaging signal and may provide better image quality in soft-tissue and low atomic number samples [1–3]. Over the last years, several PC-CT methods have been developed [4–14]. One of the recent developments is differential PC-CT (DPC-CT), based on a grating interferometer [11, 13, 15]. DPC-CT has first been implemented at x-ray synchrotron radiation sources [2, 11] and recently transferred to lab-based x-ray tube sources [16, 17]. Several experimental case studies reported in the literature demonstrate that DPC-CT offers improved soft-tissue contrast and much more internal structure details than absorption-based CT.

Most existing DPC-CT approaches are based on three kinds of scanning geometries, i.e., parallel-beam, fan-beam and cone-beam. Favored by the high imaging efficiency and the magnified spatial resolution, cone-beam DPC-CT has attracted significant interest. It includes essentially two steps: (i) retrieval of the DPC projections and (ii) phase reconstruction. The first step can be accomplished by using a phase-stepping procedure [2, 10, 11, 18], a reverse projection method [19], or a single-shot Fourier-based phase-extraction method [20]. The second step has so far been solved by using a Feldkamp-type filtered back-projection (FBP) algorithm with an imaginary Hilbert filter [16, 21].

However, while FBP-based algorithms are computationally fast and relatively easy to implement, they are known to be sensitive to incomplete datasets. If the data is truncated, the reconstruction quality can be severely degraded when simple FBP algorithms are used. This is why in absorption-based CT several attempts have been made to develop more sophisticated algorithms that can deal with data truncation. One such example is the back-projection filtration (BPF) reconstruction technique [22–25], which reconstructs the target region using truncated dataset. Recently the concept of BPF is transferred from absorption-based CT to fan-beam DPC-CT [26, 27]. This particularly exploits the fact that due to the inherent differential nature of the DPC projections, the differentiation step in the algorithm prior to back-projection can be omitted. Although BPF exhibits great advantages over FBP, there is currently no reconstruction technique to deal with incomplete datasets of cone-beam DPC-CT.

The new aspect of the work presented here is to extend the fan-beam BPF algorithm [27] to cone-beam DPC-CT, which is then applied to a numerically simulated dataset and experimentally verified using a dataset measured at a setup based on a three-grating interferometer and lab-based x-ray micro-focus source. As an additional novel aspect, we show that the simulation and experiment results demonstrate that this method can deal with several classes of truncated cone-beam DPC-CT datasets.

## 2. Materials and methods

Figure 1 displays the cone-beam DPC-CT scanning geometry. $\delta$ is the real part of the refractive index of the object, $n(x,y,z) = 1 - \delta(x,y,z) + i\beta(x,y,z)$, and proportional to the phase shift. $\alpha$ is the refraction angle. Under the para-axial approximation, the first-order derivative of the integration of $\delta$ along the incident ray direction yields the refraction angle $\alpha$. This relation can be expressed by $\alpha(x',z',\gamma) = \partial(\int_l \delta(x,y,z)dl)/\partial x' = \partial P/\partial x'$. The DPC-CT algorithms aim to reconstruct $\delta$ from the measured $\alpha$.

According to the cone-beam configuration in Fig. 2, we developed a BPF algorithm. Unlike in Fig. 1, in Fig. 2 the detector is shifted from the actual position to the rotation center. This makes the expression of the algorithm more convenient and does not affect the validity [28]. This new algorithm is expressed by

$$\delta(x,y,z) = (-1/(2\pi)) \int B(x,y,z)/(x-x')dx'. \tag{1}$$

It includes two steps: back-projection and filtering. In this formula, the image is reconstructed by applying a one-dimensional Hilbert transform on an intermediate image, which is referred to as a back-projection image $B$ and defined by

$$B(x,y,z) = \int_{\gamma 1}^{\gamma 2} \frac{1}{L(\gamma)} \frac{D\sqrt{z'^2+D^2}}{\sqrt{x'^2+z'^2+D^2}} \alpha(x',z',\gamma)d\gamma \tag{2}$$

with $L(\gamma) = \sqrt{(x-x'(\gamma))^2 + (x-y'(\gamma))^2 + (z-z'(\gamma))^2}$. The derivation of Eqs. (1) and (2) is presented in the appendix.
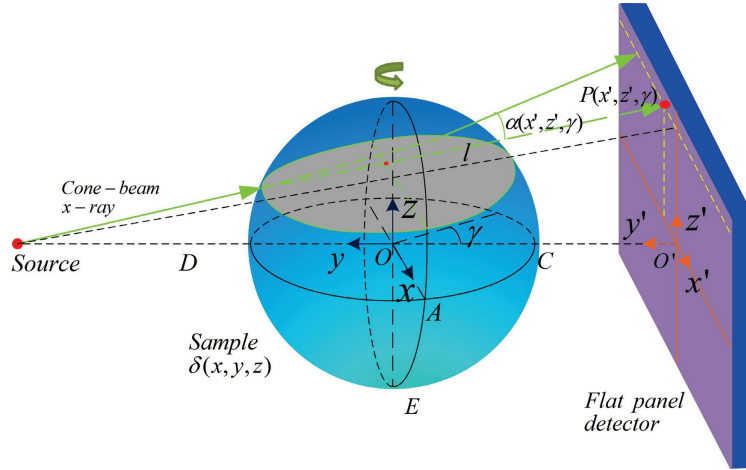
Fig. 1. Schematic geometry of x-ray refraction in a medium for cone-beam DPC-CT. $(x', z')$ represents the index of detector channel. $OAC$ is the central plane. $D$ is the distance from the source to the rotation center $O$. $\gamma$ represents the view angle under which the data was taken. $l$ is any incident ray in the three dimensional space under $\gamma$. $P$ is the line integral of $\delta$ along $l$.
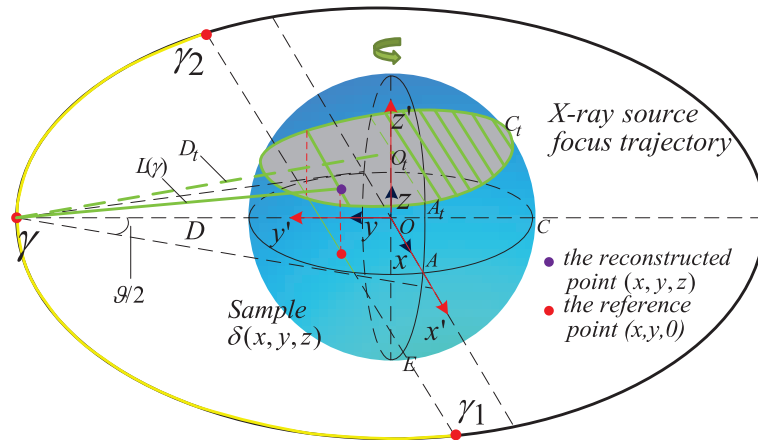


Fig. 2. Schematic representation of the cone-beam DPC-CT BPF algorithm. The sample slice in question is illustrated by green solid straight lines that are parallel to each other. $L(\gamma)$ is the distance from the reconstructed point $(x, y, z)$ to the x-ray source focus at view angle $\gamma$. $\overline{\gamma_1 \gamma_2}$ is the horizontal straight line through the reference point $(x, y, 0)$. $O_t A_t C_t$ is the tilted plane through the reconstructed point $(x, y, z)$. $D_t$ is the distance from the x-ray source focus to the rotation center $O_t$ in the tilted plane. The reconstruction of the point $(x, y, z)$ only needs the data taken in the angular range $[\gamma_1 \quad \gamma_2]$ marked by the yellow curve. $\vartheta$ is the full cone-beam angle.

The principle of this BPF algorithm is depicted in Fig. 2. The reconstructed $\delta$ is firstly treated as an image consisting of many horizontal straight lines, which are parallel to each other. Then for every reconstructed point $(x, y, z)$, its reference point $(x, y, 0)$ is fixed and the horizontal straight line through this reference point is searched in the central plane. The corresponding view angles, $\gamma_1$ and $\gamma_2$, are determined by the intersections between this horizontal straight line and the x-ray source focus trajectory. Finally back-projection and filteration operations are executed to reconstruct the point $(x, y, z)$ from data taken in the angular range $[\gamma_1 \quad \gamma_2]$.

According to the reconstruction principle, we can find the features of this algorithm depicted by Figs. 3(a)-3(d) respectively. They indicate that this algorithm has the ability to deal with the cone-beam DPC-CT data truncation. If the detector is asymmetrically placed, we can also enlarge the field of view using this algorithm.
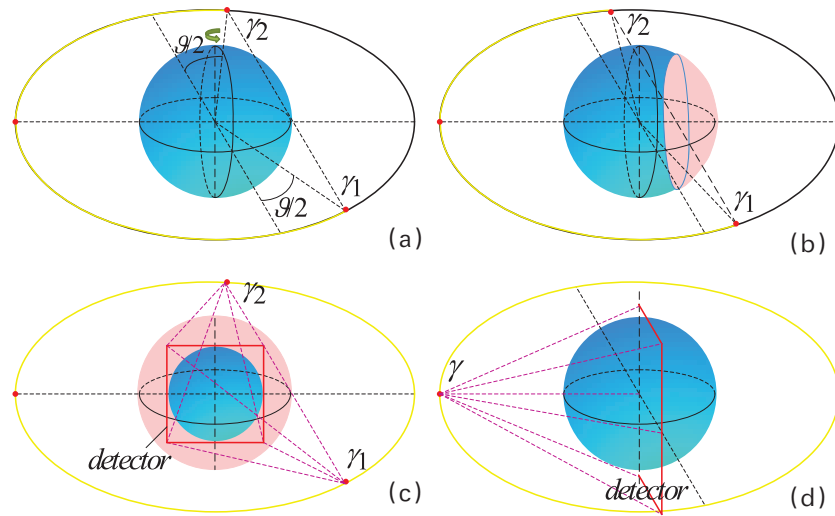


Fig. 3. Four cases of truncated data resolved by the cone-beam DPC-CT BPF algorithm. The blue regions are the areas that can be reconstructed. (a) illustrates that the entire field of view can be reconstructed if the scanning angular range is larger than $\pi + \vartheta$. (b) illustrates that a local region of interest (ROI) can be reconstructed if the scanning angular range is smaller than $\pi + \vartheta$. (c) illustrates that a local ROI can be reconstructed if the projections are truncated to a smaller view angle. (d) illustrates that the imaging field of view can be enlarged if the detector is asymmetrically placed.

Compared with the fan-beam algorithm in the reference [27], one can find that the proposed algorithm is the extension of the former one from the central plane to the tilted plane. They are consistent when the reconstructed plane is the central plane $OAC$. In this case, the value of the vertical coordinate $z$ always equals zero.

## 3. Numerical study and experiments

In order to demonstrate the validity and the above features of the method, we have carried out numerical simulations for the cases sketched in Fig. 3. The phantom used is the well-known three-dimensional Shepp-Logan head phantom [28] with a size $256 \times 256 \times 256$ pixels. Here the grey value of the phantom represents the real part of the refractive index $\delta$. $D$ is 1500 pixels and $\vartheta$ about $10°$. The scanning step angle is $1°$. In the first step, the line integral projection $P$ is calculated. Then the refraction angle $\alpha$ is derived by the three point differential method to $P$. Finally cone-beam BPF reconstructions, according to Eqs. (1) and (2), were carried out and

compared.

Figure 4 shows the simulation results for the cases in Fig. 3. We can find that Figs. 4(b) and 4(h) match the phantom well. Also the ROIs in Figs. 4(d) and (f) are consistent with the corresponding region of the phantom. Clearly, for all the mentioned truncation cases, this BPF method can reconstruct the target regions.
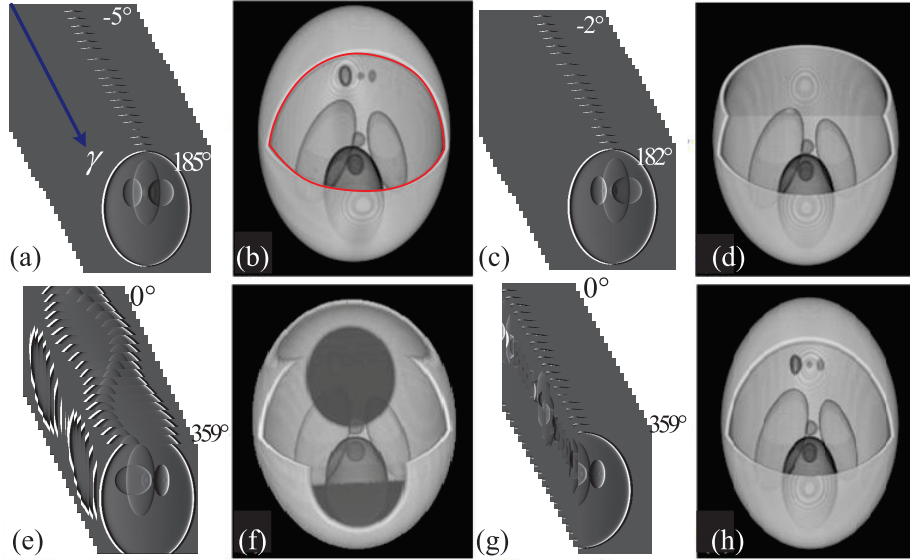


Fig. 4. Numerical simulation results for the cases in Fig. 3. (a), (c), (e) and (g) are the truncated DPC datasets with sizes $256 \times 256 \times 191$, $256 \times 256 \times 185$, $200 \times 200 \times 360$ and $138 \times 256 \times 360$ pixels respectively. (b), (d), (f) and (h) are the 3D visualization of the corresponding DPC-CT images reconstructed with the BPF algorithm that is expressed by Eq. (1). We cut some part of the sample, which is indicated by the red curves in (b), to show the internal structure.

The experimental dataset that was measured to test the BPF reconstruction algorithm was recorded at a CT setup for differential phase-contrast imaging, based on a three-grating inter-ferometer and a micro-focus x-ray tube source installed in a compact gantry at the Technische Universität München (Munich, Germany) [29]. The sample was a phantom consisting of a small plastic tube filled with spheres of different sizes and different plastic materials.

The experimental setup consisted of a tungsten x-ray source (RTW, MCBM 65B-50 W) with a focal spot size of approximately $50\mu m$ in diameter. The detector was a flat-panel sensor (Hamamatsu C9312SK-06) with $2496 \times 2304$ pixels with 50 $\mu$m square pixel size. A central area of $560 \times 1110$ pixels formed the discussed cone-beam DPC-CT geometrical configuration together with the interferometer and the x-ray generator. The cone angle was about $3.4°$ per-pendicular to the tomography axis and $6.8°$ along the tomography axis. The source-to-sample and sample-to-detector distances were approximately 270 mm and 200 mm, respectively. The gratings of the Talbot-Lau interferometer were fabricated by the company *microworks*, with grating parameters optimized for a design energy of 23 keV. The heights and periods of the grating structures were: 35 $\mu$m and $10\mu$m for the source grating $G0$, 4.0 $\mu$m and 3.2 $\mu$m for the phase grating $G1$, and 2.5 $\mu$m and 4.8 $\mu$m for the analyzer grating $G2$, respectively. The source grating was placed 31 mm from the x-ray tube. The distance between $G0$ and $G1$ was 300 mm, whereas $G1$ and $G2$ were 145 mm apart, corresponding to the first fractional Talbot distance.

The x-ray source was operated at 40 kV and 743 $\mu$A. The experimental dataset was acquired by taking 600 projections over 360° rotation, with 6 phase steps per projection and 5 seconds exposure per phase step. The projections from all the view angles provide the complete experimental dataset with a size of $560 \times 1110 \times 600$ pixels.

Sub-panels I, II, III and IV in Fig. 5 show the experimental results that are corresponding to the cases in Figs. 3(a)-3(d) respectively. In every sub-panel, the first column provides the corresponding truncated dataset generated by cropping the complete experimental dataset. The second column displays the typical axial and sagittal slices reconstructed by the algorithm expressed by Eq. (1). The third and fourth columns show the orthogonal view slices and 3D rendering of the DPC-CT images respectively. As is easily seen, sub-panels I and IV in Fig. 5 correctly display the internal structures of the phantom in the entire field of view. Sub-panels II and III correctly provide the internal structures of the phantom in the ROIs. These experimental results indicate that the field of view can be reconstructed with the BPF method if the datasets are truncated. This conclusion is the same as the one from the numerical simulation.
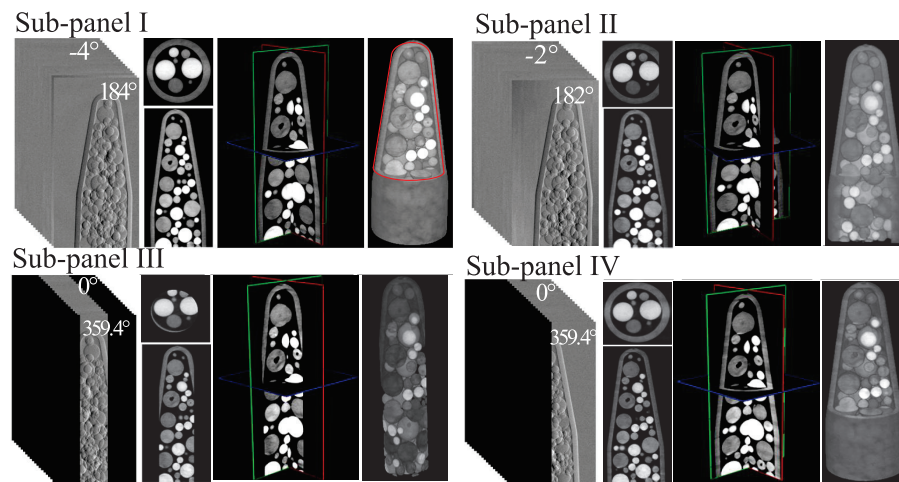


Fig. 5. Experimental results. Sub-panels I, II, III and IV are corresponding to the cases in Figs. 3(a)-3(d) respectively. First columns in sub-panels are the truncated DPC datasets with sizes $560 \times 1110 \times 315$, $560 \times 1110 \times 307$, $200 \times 1110 \times 600$ and $290 \times 1110 \times 600$ pixels respectively. Second columns display the typical axial and sagittal slices reconstructed by Eq. (1). Third and forth columns show the orthogonal view slices and 3D rendering of the DPC-CT images respectively. We cut some part of the sample, which is indicated by the red curves, to show the internal structure.

## 4. Conclusion

In summary, we have developed a BPF reconstruction algorithm for cone-beam DPC-CT configurations and demonstrated its validity both numerically and with real experimental data. This method is the extension of the recently developed BPF reconstruction algorithm for fan-beam DPC-CT [27] and can deal with several classes of truncated cone-beam datasets. It has the potential to provide a reconstruction even if the datasets are truncated. Using this feature, one can implement the DPC-CT imaging with less angular projections and consequently reduce the exposure dose. Additionally, one can also use it to enlarge the DPC-CT field of view by placing the detector asymmetrically. We envisage that, particularly for medical applications, where DPC-CT has been proven to be a uniquely powerful method, this reconstruction method will

provide a possible solution for some cone-beam imaging requirements and push x-ray DPC-CT towards future clinical applications.

## Appendix

According to Fig. 2, we have $D_t = \sqrt{D^2 + z'^2}$, $d\gamma_t \cdot D_t = d\gamma \cdot D$ and $L(\gamma) = L(\gamma_t)$. Here, $\gamma$ and $\gamma_t$ represent the rotation angular increments in the central plane $OAC$ and the titled plane $O_t A_t C_t$ respectively. So, we obtain

$$d\gamma_t = D / \sqrt{D^2 + z'^2} d\gamma. \tag{3}$$

Extending the recently developed BPF algorithm for fan-beam DPC-CT [27] to the tilted plane $O_t A_t C_t$ in Fig. 2, we will have

$$\delta(x,y,z) = (-1/(2\pi)) \int B(x,y,z)/(x-x')dx' \tag{4}$$

with

$$B(x,y,z) = \int_{\gamma 1}^{\gamma 2} \frac{1}{L(\gamma_t)} \frac{D_t^2}{\sqrt{x'^2 + D_t^2}} \alpha(x',z',\gamma)d\gamma_t. \tag{5}$$

We finally get the Eqs. (1) and (2) by replacing the corresponding variants in Eqs. (4) and (5) with $D_t = \sqrt{D^2 + z'^2}$, $L(\gamma) = L(\gamma_t)$ and Eq. (3).

## Acknowledgments

#170509 - $15.00 USD
(C) 2012 OSA

Received 13 Jun 2012; accepted 12 Aug 2012; published 5 Sep 2012
10 September 2012 / Vol. 20, No. 19 / OPTICS EXPRESS 21519